中國機械工程學刊第四十四卷第六期第 555~564 頁(民國一百一十二年)
Journal of the Chinese Society of Mechanical Engineers, Vol.44, No.6, pp555~564 (2023)

Effects of Strain Rate and Temperature on Deformation Behaviour and Microstructural Evolution of Powder Metallurgical High-speed Steel (ASP 60) Part 1 – Mechanical Behaviour

Woei-Shyan Lee* and Ting-Ju Chen **

Keywords: split-Hopkinson pressure bar, quasi-static state, work hardening, negative strain rate sensitivity, SEM fracture mechanism

ABSTRACT

The mechanical behaviour and microstructural evolution of high alloyed powder metallurgical high-speed steel ASP 60 are investigated under quasi-static and dynamic loads using an MTS 810 test machine and compressive split-Hopkinson pressure bar, respectively. The tests are performed at strain rates of 1.0×10^{-3}, 1.0×10^{-1}, 1.0×10^{0}, 2.5×10^{3}, 4.0×10^{3} and 6.0×10^{3} s^{-1} at temperatures of -195°C, 25°C, 400°C and 800°C, respectively. The effects of the strain rate and temperature on the evolution of the specimen microstructure are evaluated using optical microscopy and scanning electron microscopy. The strain rate and temperature are both shown to have a significant effect on the flow stress, work hardening behaviour, strain rate sensitivity, temperature sensitivity, and fracture mechanism. A negative strain rate sensitivity is observed at extremely high and extremely low temperatures during dynamic impacts due to the high interfacial area of the powder particles which constitute the ASP 60 microstructure. The fracture morphologies of the different specimens reveal a brittle and ductile fracture mechanism, which varies depending on the strain rate and temperature.

INTRODUCTION

ASP 60 is a high-speed steel (HSS) manufactured by a powder metallurgy process. It is widely used for cold work tooling and blanking due to its high wear resistance and compressive strength and is considered to be a practical alternative to carbide-based materials on account of its lower propensity for chipping and cracking (ASSAB Group, 2020). Compared to conventional HSSs such as M2 and the T series, which are also widely used for tool manufacture but are mostly formed using casting or wrought methods, ASP 60 contains larger amounts of special elements such as V, C, Mo, and Co. The high content of these elements yields a substantial increase in the hardness and toughness of the material, with a hardness of up to HRC 69 being achievable following appropriate heat treatment (Rong, 1992). When used in applications typical of HSS materials, such as abrasive tools and blanking thins (ASSAB Group, 2020), ASP 60 is subjected to a wide range of strain rates during the manufacturing process, including cutting (10^4 s^{-1}), drawing, stamping, forging (10^3 s^{-1}), and quasi-static deformation. The literature contains various studies on the mechanical properties of ASP 60. For example, Söderberg and Hogmark (1986) examined the wear mechanisms of ASP 60, while Gomes *et al.* (1995) discussed its fracture behaviour. Tso and Lu (1999) investigated the grinding properties of ASP 60. However, the deformation behaviour of ASP 60 under different strain rates and temperatures is still not fully clear.

The plastic deformation of ASP 60 under different strain rates and temperatures involves more than a simple change in the shape or length. For example, the mechanisms induced by dynamic impacts are substantially different from those of quasi-static deformation (Tso, 1999), (Ishikawaa, 2005), (Khan, 2012). In general, high strain rate loads result in rapid dislocation multiplication and a higher dislocation density in plastic deformation. The energy required to overcome these obstacles during dislocation glide is increased and thus a considerable work hardening effect is produced. However, adiabatic heating also plays a critical role in determining the deformation mechanism at high strain rates (Bai, 1992), and results in a deformation behaviour significantly different from that observed

Paper Received October 2023. Revised November, 2023. Accepted December, 2023. Author for Correspondence: Woei-Shyan Lee.

* *Distinguished Professor, Department of Mechanical Engineering, National United University, Miaoli, Taiwan 360302, ROC.*

***Graduate Student, Department of Mechanical Engineering, National Cheng Kung University, Tainan, Taiwan 70101, ROC.*

under quasi-static loads. At elevated temperatures, the dislocations in the impacted microstructure diffuse, and the possibility for thermally-activated dislocation motion increases. Consequently, the flow stress is reduced. As a porous material, ASP 60 also shows significantly different mechanical properties from bulk materials (da Silva, 1997). In particular, the powders which constitute the ASP 60 microstructure are nucleated from the vapor phase on the nanoscale, and hence the interfacial area in the final material is higher than that of bulk materials, and the characteristics of the mechanical properties are correspondingly changed (German, 1994).

The stress-strain properties of materials subject to high strain rate deformation tend to be rather complicated due to the competition effect between the work hardening mechanism caused by dislocation movement and the thermal softening mechanism caused by high temperature and energy. For the case of ASP 60, the situation is further complicated by the porous nature of the microstructure and the wide temperature and strain rate ranges to which it is commonly exposed in practice. Accordingly, the present study uses an MTS 810 universal testing machine and a split-Hopkinson pressure bar (SHPB) to investigate the mechanical properties and deformation substructures of ASP 60 specimens tested at strain rates ranging from 1.0×10^{-3} to 6.0×10^{3} s^{-1} and temperatures ranging from -195°C to 800°C. The microstructures of the deformed specimens are observed using optical microscopy (OM) and scanning electron microscopy (SEM). The correlation between the microstructural evolution of the ASP specimens and the mechanical response is then systematically examined and explained.

EXPERIMENTAL PROCEDURE

ASP 60 was purchased from ASSAB Co., Ltd, Taiwan with a chemical composition (wt.%) of 2.3 C, 4.2 Cr, 7.0 Mo, 6.5 W, 6.5 V and 10.5 Co. The steel was produced by the hot isostatic pressing (HIP) of gas atomized powders and was formed into plates with a thickness of 20 mm. The plates were heated at 850-900°C for soft annealing, cooled in the furnace at a rate of 10°C / h to 700°C, and then allowed to cool naturally in air. The plates were then tempered three times for 1 h at 560°C to reach a final hardness of HRC 63.10. The porosity of the ASP 60 material was determined via the Archimedes water immersion technique to be 7.8%. Figures 1(a) and 1(b) present SEM and OM images, respectively, of the ASP 60 material after the HIP process. The micrographs show clear evidence of residual pores and wide particle boundaries in the HIP microstructure.

Cylindrical specimens with a diameter and height of 7.1 mm were machined from the as-received plates by wire electrical discharge machining (WEDM). The specimens were finished by centreless grinding to a precise size of 7±0.01 mm (diameter) by 7±0.01 mm (height). The finishing process also served to remove any defects remaining on the specimen surface after WEDM processing. A compressive SHPB system was used to conduct dynamic impact tests (Lee, 2006) at strain rates of 2.5×10^{3}, 4.0×10^{3} and 6.0×10^{3} s^{-1}, respectively, under temperatures of -195°C, 25°C, 400°C and 800°C. Quasi-static state compression experiments were additionally performed using an MTS 810 universal testing machine (MTS Corp., USA) at strain rates of 1.0×10^{-3}, 1.0×10^{-1}, and 1.0×10^{0} s^{-1}, respectively, and temperatures of 25ºC and 800ºC.

Following the compression tests, the deformed microstructures were observed by OM and SEM. The OM slices were made into cold mounted samples, which were then ground sequentially using 100 to 4000 mesh abrasive papers to obtain a polished surface. The polished specimens were etched in 3% Nitral for 90 seconds, and the microstructures were then observed using a ZEISS Axiovert 200 MAT inverted microscope. The SEM specimens were washed in an ultrasonic cleaner and then dehydrated with 98% alcohol. The surface features of the specimens were then observed using a high-resolution HITACHI SU-8000 SEM.

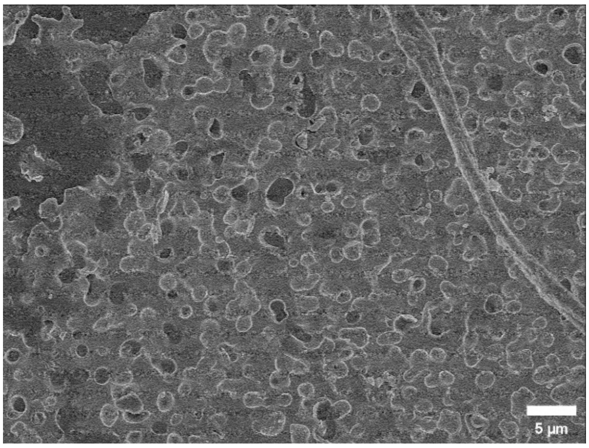

Fig. 1 (a). SEM image of undeformed ASP 60.

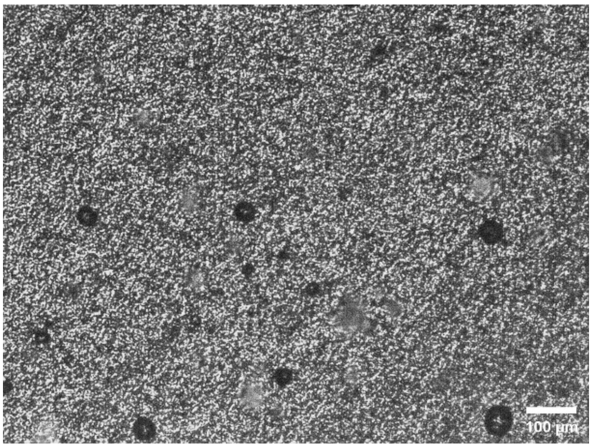

Fig. 1 (b). OM micrograph of undeformed ASP 60.

RESULTS and DISCUSSION

Stress-strain Characteristics

Figure 2 shows the typical true stress-strain curves of the ASP 60 specimens tested at temperatures of -195°C, 25°C, 400°C, and 800°C, respectively. As shown in Figs. 2(b) and 2(c), the specimens tested under dynamic strain rates at temperatures of 25°C and 400°C, respectively, show a positive dependence of the flow stress on the strain rate. However, at very low (-195°C) and very high (800°C) temperatures, the flow stress decreases with increasing dynamic strain rate, as shown in Figs. 2(a) and 2(d), respectively. In other words, the flow stress shows a negative strain rate sensitivity under high strain rates at very low or very high temperatures. For the quasi-static loading state, the flow stress also shows a negative strain rate sensitivity in the early deformation stage under room temperature conditions (25°C, Fig. 2(b)). However, at an elevated temperature of 800°C, the flow stress exhibits a positive dependence on the strain rate, as shown in Fig. 2(d). Overall, the results indicate that the tested ASP 60 specimens show both positive strain rate sensitivity and negative strain rate sensitivity under dynamic impacts and quasi-static deformation depending on the particular temperature and strain rate.

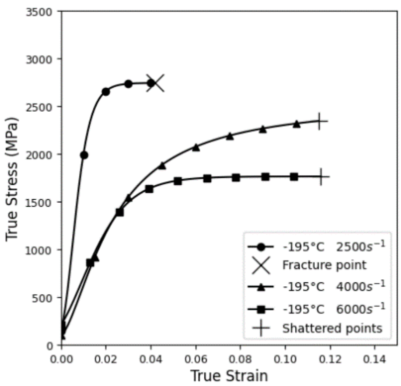

Fig. 2 (a). True stress-strain curves of ASP 60 deformed at various strain rates and temperatures of -195°C.

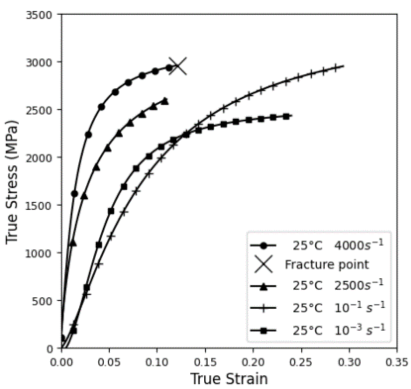

Fig. 2 (b). True stress-strain curves of ASP 60 deformed at various strain rates and temperatures of 25°C.

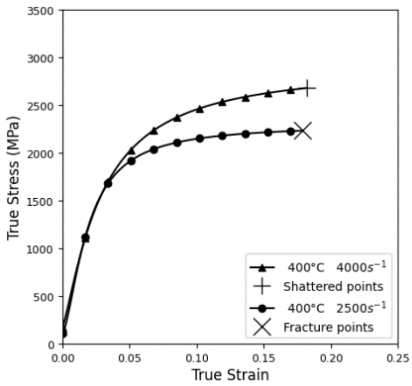

Fig. 2 (c). True stress-strain curves of ASP 60 deformed at various strain rates and temperatures of 400°C.

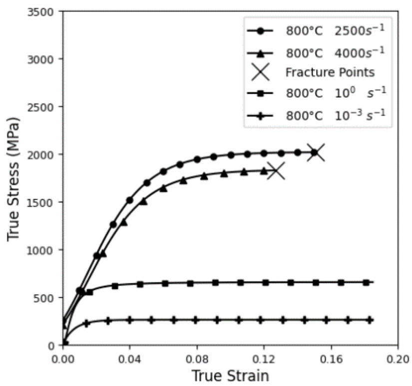

Fig. 2 (d). True stress-strain curves of ASP 60 deformed at various strain rates and temperatures of 800°C.

The negative strain rate sensitivity of ASP 60 represents a departure from the behaviour of most bulk materials (Rusinek, 2009), (Chun, 2011), (Huang, 2023) and is the result of the high interfacial area of the metallurgic microstructure. For the extremely low temperature of -195°C, the bonding areas between the particles turn brittle, leading to a lower flow resistance. Conversely, under the extremely high temperature of 800°C, the sample undergoes localized melting, resulting in an instability of the interfacial area. Consequently, the flow stress decreases with increasing strain rate, giving rise to a negative strain rate sensitivity.

As mentioned in Section 1, a higher temperature provides the dislocations with more energy to overcome local barriers to motion, and hence the flow stress reduces. However, the flow stress in the present ASP 60 specimens still exceeds 2000 MPa at 25°C and 400°C and 1500 MPa at -195°C and 800°C under high strain rates. In addition, the flow stress grows only slowly with increasing strain as a result of thermal softening. Due to the plastic work produced in compression, the work hardening effect which first dominates the deformation mechanism under dynamic and quasi-static strain rates is gradually replaced with a thermal softening effect. The final strength, therefore, reflects the outcome of a competition process between work hardening and thermal softening.

In general, the results presented in Fig. 2 indicate that the stress-strain response of ASP 60 is highly dependent on the strain rate, temperature, and strain. In particular, the ambient heat or deformation-induced energy reduces the strength of the material, while an increasing strain and strain rate lead to work hardening and an enhanced flow stress. The high interfacial area of ASP 60 further complicates the deformation mechanism and results in mechanical characteristics very different from those of bulk materials.

Work Hardening Behaviour at Different Temperatures

The work hardening rate provides a convenient means of describing the strengthening effect experienced by a material as it undergoes deformation under different strain rates and temperatures (Sohrabi, 2023), (Bortolana, 2022). Figures 3(a)~3(d) show the work hardening rates of the specimens deformed under the conditions shown in Fig. 2, where the work hardening rate is evaluated as the slope of the true stress-strain curve ($d\sigma/d\varepsilon$) in every case. In the initial compression stage, the work hardening rate has a high value for both high strain rate deformation and quasi-static deformation. However, as the strain continues to increase, the work hardening rate reduces rapidly due to thermal softening.

To better quantify the effect of work hardening, the plastic deformation process can be described by the power law $\sigma = A + B\,\varepsilon^n$, where A is the yielding stress, B is a material constant, and n is the work hardening exponent (Lee, 2011). Table 1 presents the values of A, B and n for the specimens shown in Figs. 2 and 3. (Note that the parameters were obtained in the Ludwik mode.) In general, an increase in the yielding stress (A)

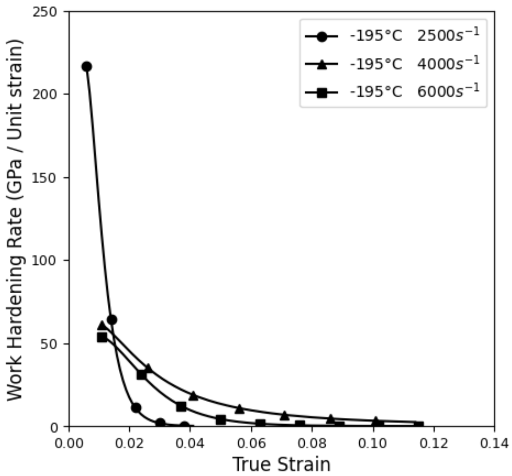

Fig. 3 (a). Work hardening rate of ASP 60 deformed at various strain rates and temperatures of -195°C.

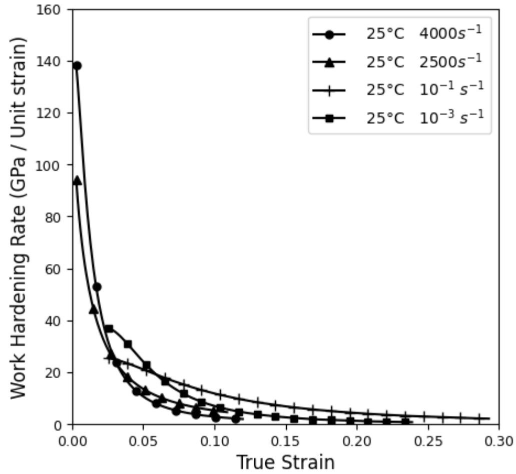

Fig. 3 (b). Work hardening rate of ASP 60 deformed at various strain rates and temperatures of 25°C.

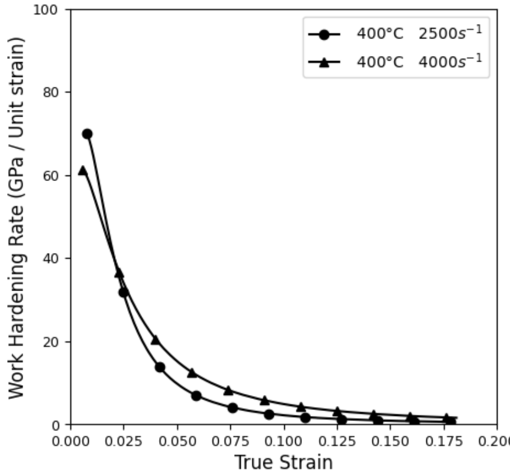

Fig. 3 (c). Work hardening rate of ASP 60 deformed at various strain rates and temperatures of 400°C.

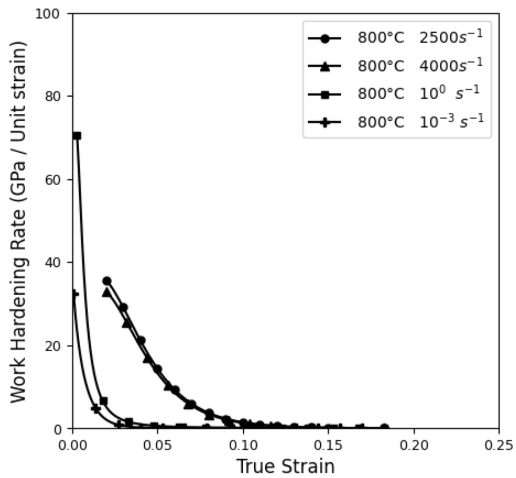

Fig. 3 (d). Work hardening rate of ASP 60 deformed at various strain rates and temperatures of 800°C.

indicates a positive strain rate sensitivity, whereas a decrease indicates a negative strain rate sensitivity. The results presented in Table 1 thus confirm that the strain rate sensitivity of ASP 60 is sensitive to changes in the yielding stress. It is additionally observed in Table 1 that the values of the work hardening exponent (n) generally exceed 0.5 (Lee, 2006), (Lee, 2005) for the considered temperature and strain rate conditions. Hence, it is inferred that ASP 60 has high formability (Doege, 2001), (Poole, 2011).

Table 1. ASP 60 material parameters obtained in Ludwik mode.

Temperature (°C)	Strain rate (s^{-1})	A (MPa)	B (MPa)	Work hardening coefficient, n
-195	2500	2533	4106	0.89
	4000	1517	7468	0.97
	6000	1447	1191	0.55
25	10^{-3}	1462	3203	0.76
	10^{-1}	1408	5629	0.98
	2500	1374	8878	0.86
	4000	1804	4736	0.62
400	2500	1536	2052	0.57
	4000	1560	4099	0.70
800	10^{-3}	226	47	0.12
	10^{0}	523	195	0.20
	2500	1497	2334	0.72
	4000	1431	1724	0.69

Figures 4 and 5 show the variation of the flow stress with the strain rate as a function of the temperature at constant strains of ε=0.04 and ε=0.08, respectively. As shown in Figs. 4(a) and 5(a), the flow stress at temperatures of 25°C, 400°C and 800°C generally increases with an increasing strain rate. However, for extreme temperatures (-195°C and 800°C) and high strain rates (2500 s^{-1}, 4000 s^{-1} and 6000 s^{-1}), the flow stress reduces under dynamic impact, as described in Section 3.1. Moreover, for constant strain rate and temperature conditions, the flow stress increases with an increasing strain. Overall, however, the results indicate that a higher strain and strain rate enhance the strength of ASP 60 as a result of work hardening.

Figures 6(a) and 6(b) show the variation of the true stress with the temperature as a function of the strain rate at constant strains of 0.04 and 0.08, respectively. For temperatures higher than 0°C, the flow stress reduces with an increasing temperature. The specimen deformed at 2500 s^{-1} shows a lower reduction in the flow stress than those deformed under any of the other considered strain rates (10^{-3} and 4000 s^{-1}).

Strain Rate Sensitivity and Temperature Sensitivity

The strain rate sensitivity is a useful measure for clarifying the dependence of the flow stress on the

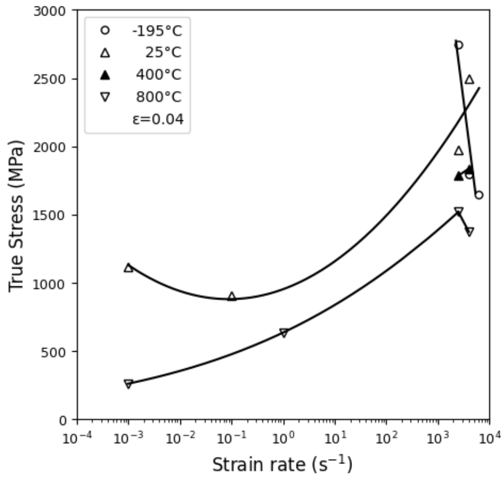

Fig. 4 (a). Flow stress as function of static and dynamic strain rate at various temperatures and constant strain of ε=0.04.

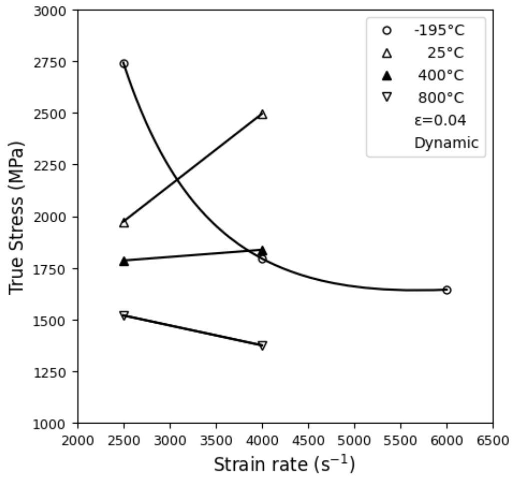

Fig. 4 (b). Flow stress as function of dynamic strain rate at various temperatures and constant strain of ε=0.04.

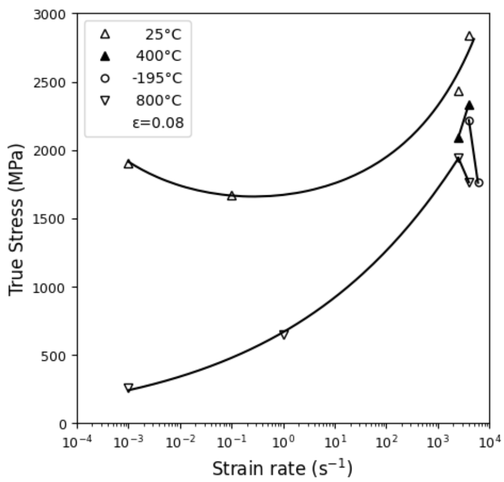

Fig. 5 (a). Flow stress as function of static and dynamic strain rate at various temperatures and constant strain of ε=0.08.

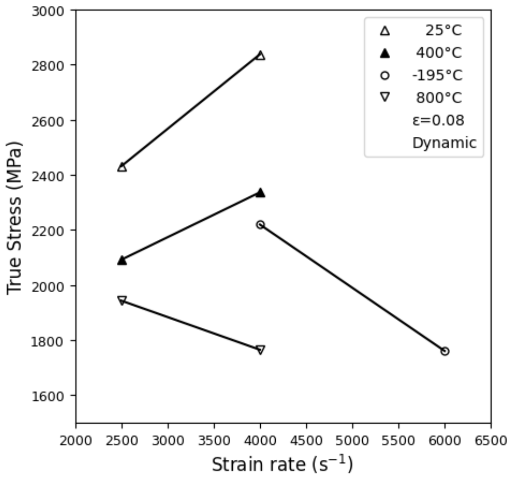

Fig. 5 (b). Flow stress as function of dynamic strain rate at various temperatures and constant strain of ε=0.08.

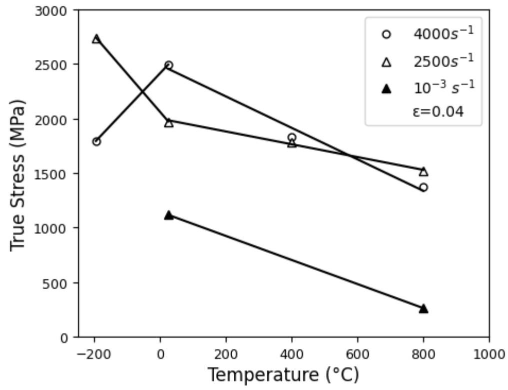

Fig. 6 (a). Flow stress as function of temperature at various strain rates and strains of ε=0.04.

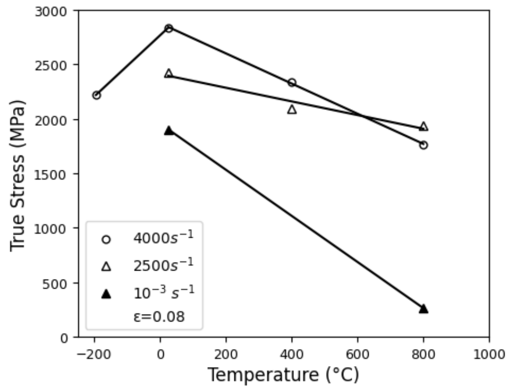

Fig. 6 (b). Flow stress as function of temperature at various strain rates and strains of ε=0.08.

change in strain rate for materials subjected to plastic deformation. The strain rate sensitivity can be defined mathematically as $\beta=(\sigma_2-\sigma_1)/\ln(\dot{\varepsilon}_2/\dot{\varepsilon}_1)$, where the flow stresses σ_2 and σ_1 are obtained at strain rates between $\dot{\varepsilon}_2$ and $\dot{\varepsilon}_1$. Table 2 shows the strain rate sensitivities of the present ASP specimens deformed at strain rates in the range of 2500 to 4000 s^{-1} at various temperatures.

Table 2. Strain rate sensitivity of ASP 60 at various temperatures.

Temperature (°C)	**Strain rate** (s^{-1})	**Strain rate sensitivity, *β*/MPa** ε=0.02	ε=0.04	ε=0.06	ε=0.08	ε=0.10
-195	2500-4000	-3165.53	-2017.41	—	—	—
25		1040.37	1110.40	992.46	864.42	752.59
400		-38.94	110.25	339.06	520.40	654.97
800		-216.90	-308.19	-356.42	-378.91	-388.66

As discussed earlier in Section 3.1, the ASP 60 samples show both positive and negative strain rate sensitivities, depending on the particular deformation conditions. For deformation temperatures of 25°C and 400°C, the ASP 60 samples have a positive strain rate sensitivity, i.e., the flow stress increases with increasing strain rate. Conversely, at extremely low and high temperatures of -195°C and 800°C, respectively, the samples show a negative strain rate sensitivity, i.e., the flow stress reduces as the strain rate increases. Also, for deformation temperatures of -195°C and 25°C, the absolute value of the strain rate sensitivity decreases with increasing strain. However, at temperatures of 400°C and 800°C, respectively, the absolute value of the strain rate sensitivity increases as the strain increases. In other words, the flow stress at elevated temperatures (400°C and 800°C) is more sensitive to changes in the strain than at low temperatures of -195°C and 25°C.

The effects of the temperature on the mechanical response of the ASP 60 specimens can be further investigated by means of the temperature sensitivity, which quantifies the change in the flow stress in response to changes in the deformation temperature. Usually, it is necessary only to consider the magnitude of the temperature sensitivity. However, due to the unusual tendencies of the strain rate sensitivity with the temperature shown by the present ASP 60 specimens, it is necessary to consider not only the magnitude of the temperature sensitivity, but also the sign. The corresponding results are presented in Table 3, where the temperature sensitivity is defined as $n_a=(\sigma_2-\sigma_1)/(T_2-T_1)$ and the flow stresses (σ_2 and σ_1) are obtained at temperatures between T_2 and T_1.

Table 3. Temperature sensitivity of ASP 60 at various strain rates.

Temperature (°C)	**Strain rate** (s^{-1})	**Temperature sensitivity, n_a (MPa/K)** ε=0.02	ε=0.04	ε=0.06	ε=0.08	ε=0.10
-195-25	2500	-5.43	-3.50	—	—	—
	4000	3.55	3.19	2.93	2.81	2.75
25-400	2500	-0.55	-0.50	-0.70	-0.91	-1.09
	4000	-1.90	-1.76	-1.52	-1.34	-1.21
400-800	2500	-0.81	-0.66	-0.43	-0.37	-0.39
	4000	-1.02	-1.16	-1.25	-1.43	-1.62

It is seen that most of the temperature sensitivity values in Table 3 have a negative sign, which indicates a loss in strength as the temperature increases. However, for temperatures in the range of -195°C to 25°C, the temperature sensitivity has a positive value at a strain rate of 4000 s^{-1}. In other words, the flow stress increases rather than decreases as the temperature rises. In general, a lower magnitude of the temperature sensitivity indicates a more moderate dependence of the flow stress on the change in temperature. For the present samples, the temperature sensitivity generally has a value greater than 0.5 and, in some cases, is greater than 1.0.

Failure Mechanisms

Table 4 illustrates the fracture morphologies and failure modes of the ASP 60 samples under different strain rates and temperatures. It is evident that the samples exhibit different fracture mechanisms depending on the particular conditions under which they were deformed. A conical fracture morphology is observed for all values of the deformation temperature, but is particularly evident for the samples tested at 25°C and 400°C. Generally speaking, fractures start from a crack or defects within the material structure, and then propagate as the deformation process proceeds. Figure 7 presents an OM image of the sample deformed at -195°C and a strain rate of 2500 s^{-1}. The pores in the microstructure develop into a crack under the effects of the applied stress, and the crack then propagates along the path of lowest fracture energy, i.e., the direction of maximum shear stress, at an angle of 45° with respect to the direction of loading. As shown in Table 4, as the temperature increases, the size of the conical shear area decreases while the area of the flat shear zone increases.

Figures 8(a) and 8(b) present SEM fractographs of the sample deformed under the highest strain rate of 6000 s^{-1} and lowest temperature of -195°C. It is seen in Fig. 8(a) that the sample has a typical brittle fracture morphology with a characteristic V-shaped chevron pattern (Callister, 2016). Notably, however, the powder particles still retain their original shape, as shown in Fig. 8(b). For room temperature conditions (25°C) and a strain rate of 4000 s^{-1}, the sample shows a mixed failure mode, with both brittle V-shaped features (Fig. 9(a)) and ductile dimple features (Fig. 9(b)). Figure 10 presents SEM fractographs of the samples tested at 400°C and strain rates of 2500 s^{-1} and 4000 s^{-1}. The radial fan-shaped ridges characteristic of brittle failure are no longer observed at a strain rate of 2500 s^{-1} (see Fig. 10(a)). However, significant cleavage features are seen in the sample tested under a higher strain rate of 4000 s^{-1}, as shown in Fig. 10(b). For the highest temperature of 800°C (Fig. 11), the samples show evidence of catastrophic fracture caused by adiabatic heating for both values of the strain rate (2500 s^{-1} and 4000 s^{-1}). Moreover, typical knobbly features associated with localized melting under the effects of intense plastic deformation are also observed (Giovanola, 1988).

In summary, the ASP 60 samples show a brittle fracture mechanism at the lowest deformation temperature of -195°C. This brittle fracture mode is replaced by a ductile fracture mechanism in the specimens deformed at 25°C. Nonetheless, a brittle

Table 4. Deformation mode and facture morphologies of ASP 60.

Temperature (°C)	**Strain rate** (s^{-1})	**State after deformation**	**Fracture morphologies** Fractured specimen	Schematic
-195	**2500**	**fractured**	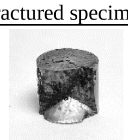 -195°C, 2500s^{-1}	
	4000	shattered		
	6000	shattered		
25	2500	deformed	 25°C, 4000s^{-1}	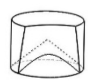
	4000	**fractured**		
400	**2500**	**fractured**	 400°C, 2500s^{-1}	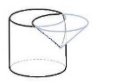
	4000	shattered		
800	**2500**	**fractured**	 800°C, 2500s^{-1}	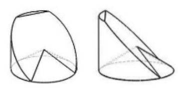
	4000	**fractured**	 800°C, 4000s^{-1}	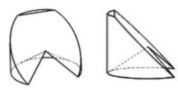

fracture mode returns when the temperature is increased to 400°C. For the highest deformation temperature of 800°C, the specimens show evidence of catastrophic fracture with knobbly features. Finally, the true stress-strain curves show that the flow stress reduces with increasing strain rate at the lowest deformation temperature of -195°C due to the low temperature brittleness effect. By contrast, at a temperature of 800°C, localized melting of the sample occurs, accompanied by interfacial instability, which leads to a reduce of flow resistance.

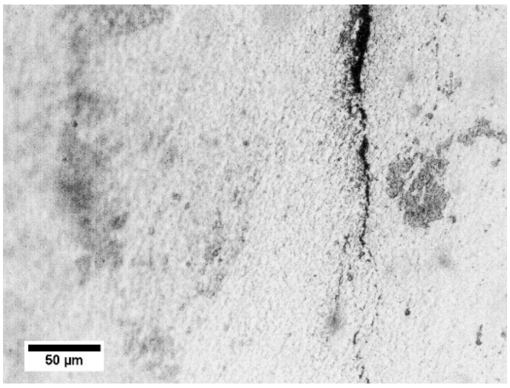

Fig. 7. OM micrograph of surface cracks of specimen deformed at -195°C and 2500 s^{-1}.

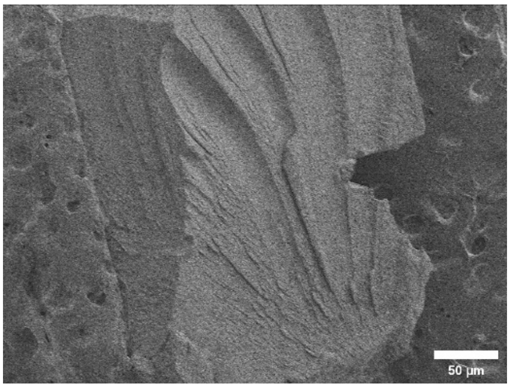

Fig. 8(a). SEM fractographs of specimens deformed at -195°C under strain rates of 6000 s^{-1}.

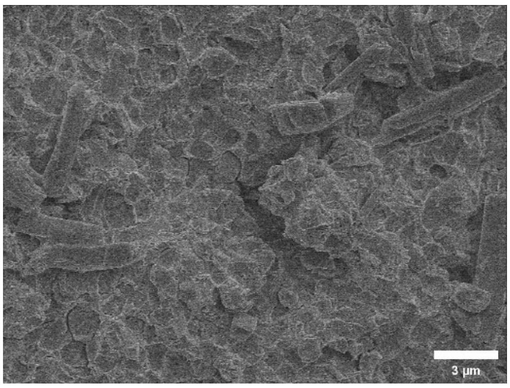

Fig. 8(b). SEM fractographs of specimens deformed at -195°C under strain rates of 6000 s^{-1}.

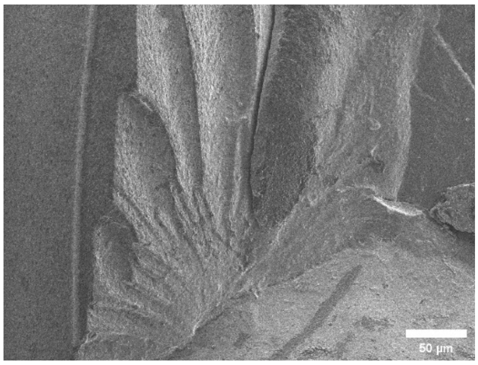

Fig. 9(a). SEM fractographs of specimens deformed at 25°C under strain rates of 4000 s^{-1}.

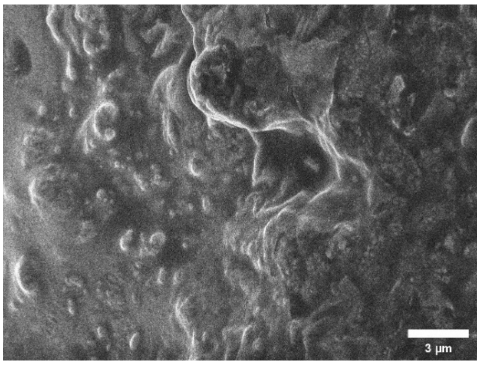

Fig. 9(b). SEM fractographs of specimens deformed at 25°C under strain rates of 4000 s^{-1}.

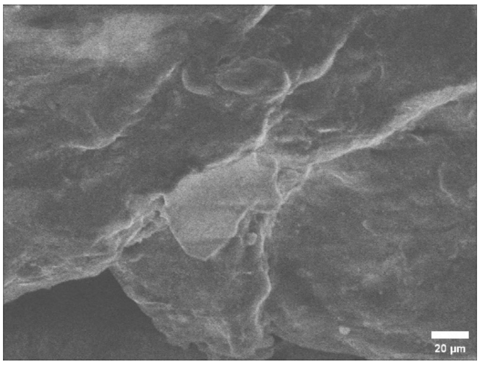

Fig. 10(a). SEM fractographs of specimens deformed at 400°C under strain rates of 2500 s^{-1}.

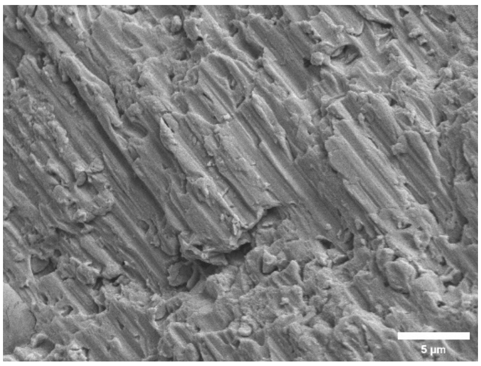

Fig. 10(b). SEM fractographs of specimens deformed at 400°C under strain rates of 4000 s^{-1}.

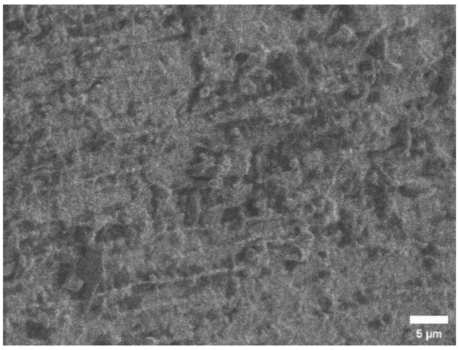

Fig. 11(a). SEM fractographs of specimens deformed at 800°C under strain rates of 2500 s^{-1}.

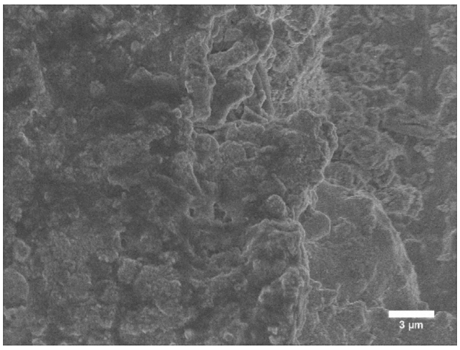

Fig. 11(b). SEM fractographs of specimens deformed at 800°C under strain rates of 4000 s^{-1}.

CONCLUSIONS

Dynamic and quasi-static compression tests have been performed to investigate the effects of the strain rate (1.0×10^{-3} s^{-1} ~ 6.0×10^{3} s^{-1}) and temperature (-195 ~ 800ºC) on the stress-strain response, work hardening behaviour, strain rate sensitivity, temperature sensitivity, and fracture mechanism of ASP 60 high-alloyed powder metallurgical high-speed steel. The results have shown that the flow stress of the ASP 60 specimens varies as a strong function of the strain rate and temperature. Both positive and negative strain rate sensitivity behaviours have been observed, depending on the deformation temperature and strain rate. The microstructural observations have suggested that the negative strain rate sensitivity stems mainly from the high interfacial area of the porous ASP 60 structure. In addition, a substantial work hardening effect has been observed under all of the considered deformation conditions. Finally, the OM and SEM observations have revealed the presence of both brittle and ductile failure modes, depending on the applied strain rate and temperature.

ACKNOWLEDGEMENTS

The authors gratefully acknowledge the financial support provided to this study by the National Science and Technology Council of Taiwan under Contract No. MOST 111-2221-E-239-018.

REFERENCES

A. Rusinek and J. A. Rodríguez-Martínez, "Thermo-viscoplastic constitutive relation for aluminium alloys, modeling of negative strain rate sensitivity and viscous drag effects," *Mater. Des.*, vol. 30, pp. 4377–4390, 2009.

A. S. Khan, M. Baig, S. H. Choi, H. S Yang and X. Sun, "Quasi-static and dynamic responses of advanced high strength steels: Experiments and modeling," *Int. J. Plasticity*, vol. 30-31, pp. 1-17, 2012.

ASSAB Group, "ASSAB ASP 60 Datasheet", URL: http://cdna.terasrenki.com/ds/1.3241_1.3292_HS6-7-6-10_SS-2727_Vanadis_60_ASP-60_Datasheet_1.pdf, (accessed 2020-05-25).

C. C. Bortolana, L. C. Campanellib, P. Menguccic, G. Baruccac, N. Giguèred, N. Brodusche, C. Paternostera, C. Bolfarinif, R. Gauvine and D. Mantovania, "Development of Ti-Mo-Fe alloys combining different plastic deformation mechanisms for improved strength-ductility trade-off and high work hardening rate," *J. Alloy Compd.*, vol. 925, p. 166757, 2022.

C. P. Huang, M. Wang, K. Y. Zhu, A. Perlade and M. X. Huang, "Carbon-induced negative strain-rate sensitivity in a quenching and partitioning steel," *Acta Mater.*, vol. 255, p.119099, 2023.

E. Doege and T. Hallfeldt: Encyclopedia of Materials, Science and Technology (Second Edition), pp. 5518-5521, 2001.

J. H. Giovanola, "Adiabatic shear banding under pure shear loading part II: fractographic and metallographic observations," *Mech Mater.*, vol. 7, pp. 73-87, 1988.

K. Ishikawaa, H. Watanabea and T. Mukaib, "High strain rate deformation behavior of an AZ91magnesium alloy at elevated temperatures," *Mater. Lett.*, vol. 59, pp. 1511-1515, 2005.

M. A. Gomes, A. S. Wronski and C. S. Wright, "Fractue behaviour of a highly alloy high speed steel," *Fatigue Fract. Engng. Mater. Struct.*, vol. 18 pp. 1-18, 1995.

M. G. da Silva and K. T. Ramesh, " The rate-dependent defornation and locaization of fully dense and porous Ti-6Al4V," *Mater. Sci. Eng. A.*, vol. 232, pp.11-22, 1997.

M. J. Sohrabi, H. Mirzadeh, S. Sadeghpour and R. Mahmudi, "Explaining the drop of work-hardening rate and limitation of transformation-induced plasticity effect in metastable stainless steels during tensile deformation," *Scr. Mater.*, vol. 231, p. 115465, 2023.

P. L. Tso and C. C. Lu, "Study on the grinding of P/M high speed steel ASP 60," *Int. J. Mach. Tools Manuf.*, vol. 39, pp. 627–638, 1999.

R. M. German, Powder Metallurgy Science, pp. 150-151, 1994.

S. A. Habib, C. S. Meredith and A. S. Khan, "Quasi-static and dynamic investigation of an advanced high strength and corrosion resistant 10 % Cr nanocomposite martensitic steel," *Int. J. Mech. Sci.*, vol. 211, p. 106774, 2021.

S. Söderberg and S. Hogmark, "Wear mechanisms and tool life of high speed steels related to microstructure," *Wear*, vol. 110, pp. 315 - 329, 1986.

W. D. Callister, Jr. and D. G. Rethwisch, Fundamentals of Materials Science and Engineering: An Integrated Approach, (John Wiley & Sons Inc., New York, 2016) pp. 326-329, 2016.

W. J. Poole, J. D. Embury and D. J. Lloyd, Fundamentals of Aluminium Metallurgy, 11 - Work hardening in aluminium alloys, (Woodhead, Cambridge ,2011) pp. 307-344, 2011.

W. Rong, H. O. Andren, H. Wisell and G. L. Donlup, " The role of alloy composition in the precipitation behaviour of high speed steel," *Acta Metall. Mater.*, vol. 40, pp. 1727-1738, 1992.

W. S. Lee, C. F. Lin, T. H. Chen and H. W. Chen, "Dynamic mechanical behaviour and dislocation substructure evolution of Inconel 718 over wide temperature range," *Mater. Sci. Eng. A.*, vol. 528, pp. 6279–6286, 2011.

W. S. Lee and C. H. Hsu, "Dependence of impact deformation behaviour of Fe–2Ni sintered alloy on strain rate and sintered density," *Mater. Sci. Technol.*, vol. 22, pp.1431-1443, 2006.

W. S. Lee and C. Y. Liu, "The effects of temperature and strain rate on the dynamic flow behaviour of different steels," *Mater. Sci. Eng. A.*, vol. 426, pp. 101–113, 2006.

W. S. Lee and J. K. Chou, "The Effect of Strain Rate on the Impact Behaviour of Fe–2 mass% Ni Sintered Alloy," *Mater. Trans.*, Vol. 46, pp. 805-811, 2005.

Y. Bai and B. Dodd, Adiabatic Shear Localization: Occurrence, Theories and Applications, p.1, 1992.

Y. B. Chun and C. H. J. Davies, "Twinning-induced negative strain rate sensitivity in wrought Mg alloy AZ31," *Mater. Sci. Eng. A.*, vol. 528, pp. 5713–5722, 2011.

應變速率及溫度在粉末冶金高速鋼(ASP 60)變形行為與微觀結構上的效應分析 Part 1—機械性質

李偉賢
國立聯合大學機械工程學系

陳亭儒
國立成功大學機械工程學系

摘要

本研究分別透過MTS 810萬能材料試驗機及霍普金森撞擊試驗機(SHPB)，研究粉末冶金高速鋼(ASP 60)於準靜態(quasi-static)及動態荷載(dynamic load)下的變形行為，並使用光學顯微鏡(OM)和掃描電子顯微鏡(SEM)觀察材料微觀形貌變化，釐清應變速率和溫度如何影響粉末冶金高速鋼(ASP 60)之機械性質。本實驗條件為：應變速率1.0×10^{-3}、1.0×10^{-1}、1.0×10^{0}、2.5×10^{3}、4.0×10^{3}、6.0×10^{3} s^{-1}，及溫度-195°C、25°C、400°C、800°C。實驗結果顯示，應變速率和溫度皆大幅影響粉末冶金高速鋼(ASP 60)之塑流應力、加工硬化行為、應變速率敏感性係數、溫度敏感性係數及破壞機制。且由於材料內部之粉末冶金顆粒組成特性，粉末冶金高速鋼(ASP 60)於極高溫和極低溫下的動態變形皆出現負應變率敏感性現象。觀察試件斷裂之形貌可發現，隨應變率和溫度變化，粉末冶金高速鋼(ASP 60)分別呈現脆性、韌性不同的破壞機制。